Prediction of Potential Urban Hot Spots in Urban Environments Using Convolutional Neural Networks and Remote Sensing Techniques

Jiongye Li[1], Rudi Stouffs[1]

[1] Department of Architecture, College of Design and Engineering, National University of Singapore, 4 Architecture Dr, 117566, Singapore - lijiongye@u.nus.edu, stouffs@nus.edu.sg

Keywords: Urban Hot Spots, Land Surface Temperature, Deep Learning, Remote Sensing, Prediction.

Abstract

With the increase in built-up areas and rising urban populations, Land Surface Temperature (LST) has significantly increased, leading to the proliferation of Urban Hot Spots (UHS) in urban environments. To mitigate UHS proactively, researchers have conducted studies using various models to predict LST. However, current predictions are primarily based on data samples from isolated stations, making them unfeasible for continuous LST prediction on larger scales, such as regional levels. Therefore, this research aims to use Singapore as a case study to predict UHS on a regional scale using machine learning based on essential variables. Specifically, this research proposes training a Convolutional Neural Network (CNN) model using identified independent variables, including elevation, Normalized Difference Built-up Index (NDBI), Normalized Difference Moisture Index (NDMI), Normalized Difference Vegetation Index (NDVI), Normalized Difference Water Index (NDWI), population, and Land Use and Land Cover (LULC), along with the target variable, UHS. After training, the model achieves high test accuracy and is fed projected data, subsequently producing projected UHS locations. The findings indicate that new UHS primarily appear in southwestern areas, Marina Bay, and the northwest regions of the country. This research predicts that 2.24 percent of the site could be classified as UHS by 2025, compared to the current percentage of 0.95 percent. Based on these projections, the research proposes preventative measures to proactively mitigate UHS. This research fills the gap by constructing a prediction model that can predict UHS locations on a regional scale.

1. Introduction

Urban Hot Spots (UHS) refer to high-temperature areas within Urban Heat Islands (UHI) that can cause extreme heat stress, impacting people’s activities (Guha et al., 2018; Pearsall, 2017). The focus on UHS differs from UHI, as UHI primarily concerns the difference between the air and Land Surface Temperature (LST) in urban and nearby rural areas (Krtalić et al., 2020). In contrast, UHS, within the urban context, is more closely related to people’s health, specifically the level of heat stress experienced (Kuang et al., 2014; Guha, 2017). UHS are found in areas with higher values of UHI and LST (Das and Das, 2020). Therefore, with the rapid increase of LST in urban areas in recent years, the amount of UHS is also booming, as validated by researchers in various regions globally (Ahmed, 2018; Amindin et al., 2021). Additionally, the correlation between UHS and LST has been further precisely interpreted by Guha et al. (2017) through a mathematical formula. Thus, it is safe to say that the locations of UHS are based on the values of LST.

The values of LST have been found to correlate with urban morphology, Local Climate Zone (LCZ), spectral indices from satellite imagery, land use and land cover, and demographic factors (Zeng et al., 2023). Specifically, regarding urban morphology, researchers have found that trees can effectively reduce LST and that irregular distribution and diverse species of green spaces can reduce LST more effectively (Huang and Wang, 2019). Additionally, concerning building layout, Huang et al. (2019) found that high-rise buildings scattered in location could reduce LST more effectively. Furthermore, in terms of insights from satellite imagery, the Normalized Difference Vegetation Index (NDVI) is found to be negatively related to LST value, and the Normalized Difference Built-up Index (NDBI) is positively related to LST value (Guha et al., 2018; Zhang et al., 2009). Researchers have also found that different land uses and land covers impact LST properties differently, and changes in land use due to rapid urbanization can lead to changes in LST (Kardinal et al., 2007). Specifically, commercial and industrial land uses typically have high LST during the daytime (Huang and Wang, 2019; Kardinal et al., 2007). Furthermore, in terms of the demographic aspect, researchers have found that higher population density generally represents higher traffic volume and thus results in higher LST (Bokaie et al., 2016).

Researchers have also conducted predictions of LST to identify future UHS and mitigate their impact in advance (Equere et al., 2020; Khalil et al., 2021). Advanced machine learning algorithms, such as Artificial Neural Network (ANN) and Convolutional Neural Network (CNN) models, fed with LST values and necessary independent variables, have shown higher accuracy than linear regression models in predicting LST (Deo and Şahin, 2017; Equere et al., 2021; Khalil et al., 2021). Deo et al. (2017) used training and testing data from seven sites to compare the accuracy of different models, including ANN, Multiple Linear Regression (MLR), and Autoregressive Integrated Moving Average (ARIMA) algorithms, and found that ANN has the highest accuracy. Similarly, Equere et al. (2021) randomly selected pixels from a region to train and validate their model for predicting future LST. However, these predictions of LST are limited to certain pixels or sites, making the method time-consuming for larger regions. In summary, to the best of our knowledge, current research mainly focuses on predicting LST values, rather than UHS, and is often based on selected points within research sites.

With the urgency to mitigate potential future UHS and the proven high accuracy of machine learning in estimating LST trends, this research aims to utilize machine learning techniques for

This contribution has been peer-reviewed. The double-blind peer-review was conducted on the basis of the full paper.
https://doi.org/10.5194/isprs-annals-X-4-2024-195-2024 | © Author(s) 2024. CC BY 4.0 License.

predicting potential UHS locations on a regional or national scale, based on factors correlated with UHS. Compared to UHI, UHS is an index more directly related to people’s experience of heat stress (Coutts et al., 2015). Building upon current research, which mainly focuses on predicting LST and UHI, the results of this study will fill the research gap in predicting UHS using machine learning models, thereby making the research field more complete. Additionally, the outcomes of this research could be utilized by urban planners to implement mitigation solutions in advance to prevent the increase of UHS.

2. Research Site and Data

2.1 Research Site

Singapore, situated near the equator at 1°17’ N, 103°50’ E, as shown in Figure 1, is characterized by a tropical climate, which has similar climate settings for all seasons. Singapore covers an area of 734.3 km² and with a population of 5.92 million as of June 2023. The region maintains a consistent climate with average temperatures ranging from 26.8°C to 28.6°C. Daily highs vary from 30.5°C to 32.4°C, and lows from 24.3°C to 25.7°C (The National Environment Agency). Research indicates a potential temperature increase due to urbanization of up to 0.79°C by the 2030s and an additional 2.3°C by the 2080s (Zhu and Yuan, 2023). Owing to the lack of data regarding Tekong Island, this research excludes Tekong Island from its scope.

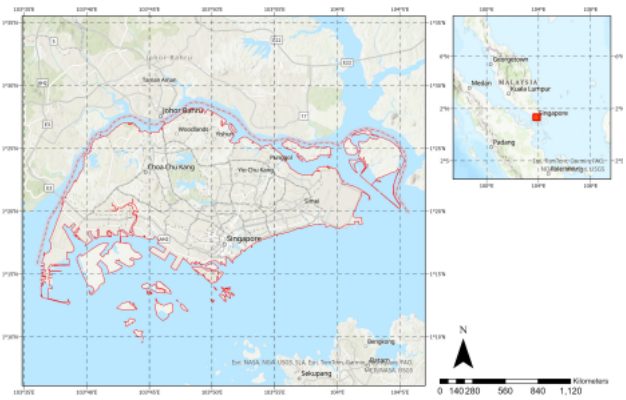

Figure 1. Research site geographic location.

2.2 Data

This research utilizes data from three primary sources: Digital Elevation Model (DEM) data from the National Aeronautics and Space Administration (NASA), Landsat 8 data from the United States Geological Survey (USGS), LULC data from Senti -nel-2 land cover, and demographic data from the Singapore Department of Statistics (DOS). The DEM data from NASA reveals the bare surface of the research site with a resolution of 30 m by 30 m. The Landsat 8 Collection 2 Level 1 dataset from October 13, 2023, was selected for its recency and minimal cloud coverage. This research employs five bands from the Landsat 8: GREEN (Band 3), RED (Band 4), NIR (Near-Infrared, Band 5), SWIR1 (Short-Wave Infrared 1, Band 6), and Thermal Infrared (Band 10). The third dataset, detailing the LULC of Singapore in 2017 and 2022, is obtained from Sentinel-2 land cover. The fourth dataset, detailing the population of Singapore in 2022, is obtained from DOS. The population data are categorized by subzone, which is a subdivision of Singapore’s planning zones. Table 1 describes the data, its resolution, the time of collection, and its sources.

Data	Resolution	Time	Sources
DEM	30 m	2019	NASA
Landsat 8 (Band 3, 4, 5, 6 and 10)	30 m and 100 m	Oct 13, 2023	USGS
LULC	10 m	2017, 2022	Sentinel-2 land cover
Population	subzone	2022	DOS

Table 1. Descriptions of data, data resolution and data sources in the research.

3. Methodology

Figure 2 illustrates the general method applied in this research. Independent variables, including elevation, NDBI, NDMI, NDVI, NDWI, population, and LULC, are converted into a multi-channel array. The target variable, which is the current UHS, is transformed into one-hot encoded matrices. After the CNN model is trained using the training dataset comprising independent variables and target variables, it is fed projected independent variables, and subsequently, it produces a projected UHS. More details regarding the model will be explained in Section 3.3.

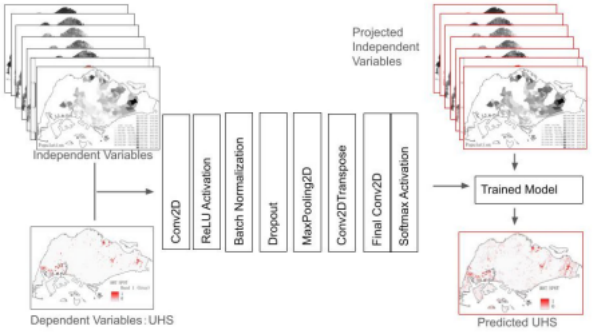

Figure 2. Diagram of general research method.

3.1 Retrieval of Independent Variables

Major contributing factors of urban heat have been identified by Voogt and Oke in 2008, including geographic location, time, weather conditions, city function, city size, and city form (Voogt, 2008). The research location, city size, weather, and time are set in the research site section and will not be subjected to change, and thus are not recognized as independent variables. Therefore, this research focuses on applying impacting factors from the city function and city form categories to predict the UHS in the research site. Based on a comprehensive literature review, Rajagopal (2023) summarized the specific impacting factors of urban heat regarding city function and city form that were used by researchers in the past ten years (Rajagopal et al., 2023). Wang et al. (2023) conducted a critical literature review regarding the prediction of air temperature in the past ten years and summarized the frequently used variables in predicting air temperature (Wang et al., 2023). Based on the frequency of relevance of the impacting factors in the above two literature reviews, this research identified seven crucial independent variables, including elevation, NDBI, NDMI, NDVI, NDWI, population and LULC, that will be applied in our research. Specifically, surface elevation has been proven to be a significant factor

that can improve the accuracy of LST prediction (Equere et al., 2020). NDBI, which indicates built-up areas, has been found to have a positive correlation with LST values. In contrast, NDVI, which evaluates vegetation percentage, and has been found to be negatively correlated with LST (Kumar et al., 2022). Furthermore, NDMI, describing the water stress level in vegetation, and NDWI, mapping the index for water bodies, have also been found to correlate with LST values (Taloor et al., 2021). The density of population, indicating the level of activities of residents which can potentially generate anthropogenic heat in urban areas, has been found to be positively correlated with LST in residential regions (Li et al., 2014). Finally, different LULC types have been found are associated with levels of LST by researchers (Halder et al., 2021).

NDBI is calculated from the NIR and SWIR1 bands, which are bands 5 and 6, via equation(Zha et al., 2003):

$$NDBI = \frac{(SWIR1 - NIR)}{(SWIR1 + NIR)} \tag{1}$$

NDMI is calculated as the ratio between the difference and the sum of the refracted radiations in the NIR and SWIR regions (Gao, 1996). The formula is:

$$NDMI = \frac{(NIR - SWIR1)}{(NIR + SWIR1)} \tag{2}$$

The NDVI is calculated as the ratio of the difference between the NIR and RED reflectance to the sum of these two values (Purevdorj et al., 1998). Its equation is:

$$NDVI = \frac{(NIR - RED)}{(NIR + RED)} \tag{3}$$

NDWI is calculated using the Green and NIR bands (Mcfeeters, 1996), as follows:

$$NDWI = \frac{(GREEN - NIR)}{(GREEN + NIR)} \tag{4}$$

This research also use two projected independent variables, which are projected population of 2025 and projected LULC of 2025. Specifically, Singapore's population is projected to increase to 6.9 million in 2030, up from the current 5.92 million (Singapore Department of Statistics, 2023), resulting in an increase rate of 16.9 percent. Based on this rate, the research projects that the population of each subzone will increase by 4.82 percent in 2025. This change in population for each subzone is represented by variations in color within an image format.

Regarding projected LULC, the Modules for Land Use Change Simulations (MOLUSCE) employs multiple models and algorit -hms, including Cellular Automata (CA), ANN, and Logistic Regression (LR), based on necessary inputs such as previous land use maps and distance to road systems, and has been proven to have high accuracy in simulating future land use (Muhammad et al., 2022). MOLUSCE can be implemented via QGIS to simulate the predicted LULC map for 2025 based on the LULC maps of 2017 and 2022, and the road system of 2022. Firstly, the model will predict the LULC of 2022, which will be compared with the LULC map of 2022 from Sentinel-2 land cover data. The two LULC maps are compared to validate the model's accuracy using the kappa value, which is calculated via formula:

$$K = \frac{P_o - P_e}{1 - P_e} \tag{5}$$

where K = The Kappa coefficient
P_o = Probability of observed agreement
P_e = Probability that agreement between the observed and predicted data occurs by chance

The value of the Kappa coefficient varies from -1 to 1, with higher values indicating better performance in predicting the LULC map. Once the model is trained to achieve sufficient accuracy, it will be used to predict the LULC of 2025.

3.2 Retrieval of the Dependent Variable

LST can be retrieved using the methods provided by (Yuan and Bauer, 2007). The computation of Top of Atmospheric (TOA) spectral radiance utilizes Band 10 of the Landsat 8 data. TOA radiance is calculated using the formula:

$$\text{TOA} = ML \times Qcal + AL - Oi \tag{6}$$

where ML = Radiance Multiplicative Scaling Factor
AL = Radiance Additive Scaling Factor
$Qcal$ = Quantized calibrated Digital Number (DN)
Oi = Correction factor, set at 0.29

This process is followed by converting TOA radiance to Brightness Temperature (BT) using the equation:

$$BT = \frac{K2}{\ln\left(\frac{K1}{TOA} + 1\right)} - 273.15 \tag{7}$$

where $K1, k2$ = Thermal band-specific conversion constant

The resulting temperature, initially in Kelvin, is converted to Celsius by subtracting 273.15.

Subsequent to this, NDVI was calculated using the formula:

$$NDVI = \frac{NIR - Red}{NIR + Red} \tag{8}$$

with NIR and Red representing the spectral reflectance in the near-infrared and red wavelengths, respectively. NDVI is crucial for correcting emissivity in the LST calculation.

where NIR = Spectral reflectance in near-infrared wavelengths
Red = Spectral reflectance in the red wavelengths

The Proportion of Vegetation (Pv) was estimated from NDVI through the equation:

$$Pv = \left(\frac{NDVI - NDVI_{min}}{NDVI_{max} - NDVI_{min}}\right)^2 \tag{9}$$

where $NDVI_{min}$ = Minimum observed NDVI value
$NDVI_{max}$ = Maximum observed NDVI value

The surface emissivity (ϵ) was calculated using the formula:

$$\epsilon = 0.004 \times Pv + 0.986 \tag{10}$$

where ϵ = Land Surface Emissivity
Pv = Proportion of Vegetation

Finally, LST was calculated using the equation:

$$LST = \frac{BT}{1 + (\lambda \times BT/C2) \times \ln(\epsilon)} \tag{11}$$

where λ = Wavelength of emitted radiance
$C2$ = Second radiation constant, valued at 14,388 $\mu m \cdot K$
λ = 10.8 μm for Band 10
λ = 12.0 μm for Band 11

Finally, the dependent variable in this research, Urban Hot Spots, are identified using the formula proposed by Guha et al. (2017):

$$LST > T_{mean} + 2 \times StdDev \tag{12}$$

where T_{mean} = Mean LST
StdDev = Standard deviation of LST

Applying this formula, this study will pinpoint urban hot spots in the research site.

3.3 Predicting Future UHS by CNN Model

The prediction process based on the CNN model can be divided into four parts: data preparation, training, evaluation and prediction. Firstly, regarding data preparation, this research processes all variables, including LST, elevation, NDBI, NDMI, NDVI, NDWI, population, and LULC data, into 8 uniformly sized images of 2827 by 4000 pixels. The independent variables are subsequently transformed into a multi-dimensional array, where each channel corresponds to an input variable, with the exception of LULC, which utilizes three channels to represent its RGB values. The target variable, the UHS diagram, is converted into one-hot encoded matrices for classification purposes. Both independent and dependent data are split into training data (80 percent) and testing data (20 percent).

Next, the training data is fed into the model. The model architecture consists of 6 layers. The first Conv2D layer has 20 filters to extract spatial features from the input data. The second batch normalization layer normalizes activations from the previous layer. A dropout layer, setting a portion of inputs to zero during training, helps prevent overfitting. Max pooling is used to reduce the dimension of the input, followed by a Conv2D transpose layer for upsampling. The final layer, a Conv2D layer with 2 filters, classifies each pixel into one of two classes. The model is updated using the Adam optimizer and the categorical cross-entropy loss function, over 7 epochs and a batch size of 10. Finally, the trained model is tested on the split testing data and evaluated based on test accuracy. The test accuracy is calculated as the percentage of accurately predicted classes for pixels divided by the total pixels of the dependent variable, and the formula is shown as follows:

$$Accuracy = \frac{NumberofCorrectPixels}{TotalNumberofPixels} \tag{13}$$

After training the model to achieve sufficient accuracy, this research feeds the model with projected independent variables to predict future UHS. In this study, we use one projected variable, the projected LULC and population of 2025, while keeping other input variables unchanged, to assess how future LULC and population trends may impact UHS.

4. Result

4.1 Retrieval of Independent Variables

Figure 3, 4, 5, 6, 7, 8, and 9 show the independent variables of current situation, including elevation, NDBI, NDMI, NDVI, NDWI, LULC, and population. All images are under the EPSG: 4326 - WGS 84 coordinate reference system (CRS). The elevation diagram indicates that high elevation areas in the research are primarily concentrated in the central region. The NDBI diagram reveals that green spaces and water bodies in the central water catchment and western areas have a relatively lower NDBI index than other built-up areas. Conversely, NDMI shows that green spaces in central and western water catchment areas have relatively higher values than built-up areas. Similarly, the NDVI index is high for green spaces in central and western areas, while water bodies and built-up areas belong to low NDVI index ranges. Water bodies, like rivers, have a relatively high NDWI index, as indicated in the diagram. The population diagram, as denoted by the shade of color, reveals that most people are concentrated in the eastern, southeastern, and northern areas of the country. This observation aligns with findings from other related research (Li et al., 2023). The LULC diagram, as denoted by the legend, reveals the distribution of vegetation, built areas, trees, water bodies, crops, and bare ground, which refer to infrastructure in the context of Singapore.

Figure 12 and 13 and show the predicted independent variables, including LULC of 2025 and population of 2025. The optimal parameters set in the MOLUSCE model to predict LULC include: sample mode set to ’random’, the number of samples to ’1000’, method set to ’Artificial Neural Network (Multi-layer Perceptron)’, neighborhood to ’1px’, learning rate to ’0.100’, maximum iterations to ’1000’, and hidden layers to ’10’. After training, the accuracy of the predicted LULC map of 2025 is validated by a high Kappa value which is 0.85, indicating 85 percent correctness when comparing the predicted LULC map of 2022 with the existing LULC map of 2022.

4.2 Retrieval of Dependent Variables

Figure 10 displays the retrieved LST values. In this research, the range of LST values is divided into five categories, each indicated by different colors. As shown in the diagram, blue and green colors represent areas with higher LST, over 32.43 degrees Celsius, while orange and grey colors denote areas with relatively lower LST values. UHS, depicted in Figure 11, is retrieved based on equation 12 from the LST diagram. The

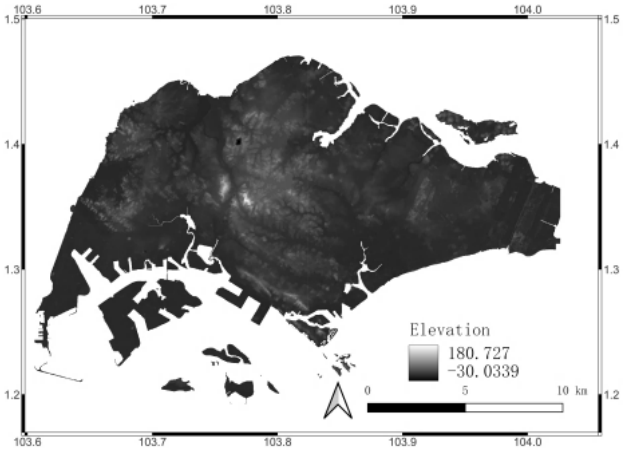

Figure 3. Elevation of the research site based on DEM from NASA. Unit: meters.

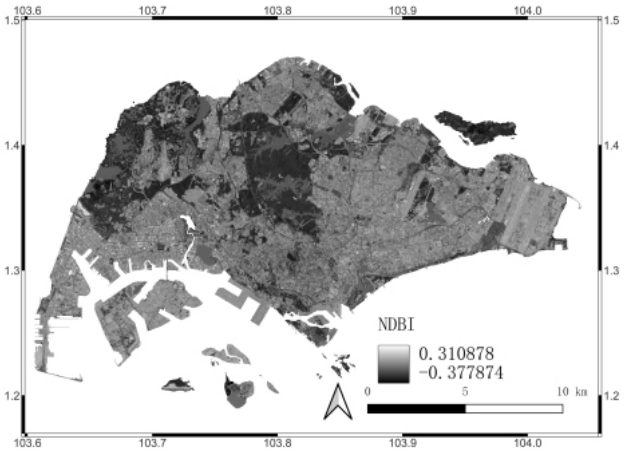

Figure 4. NDBI of the research site based on Landsat 8 satellite imagery.

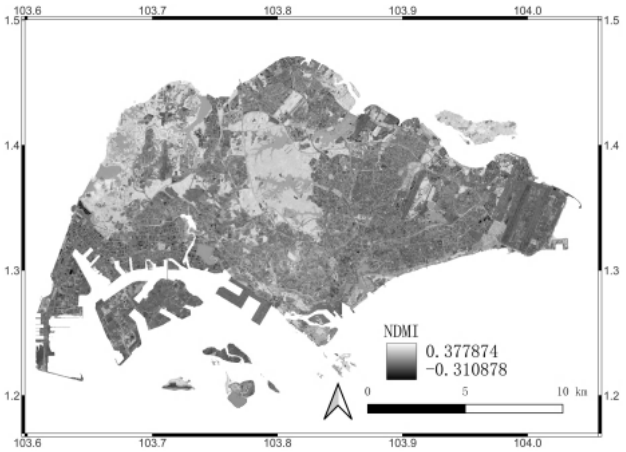

Figure 5. NDMI of the research site based on Landsat 8 satellite imagery.

values of UHS are shown in binary format, meaning that a value of 1 indicates the location of UHS, while a value of 0 indicates that there is no UHS. According to the UHS diagram, these spots are primarily concentrated in the eastern, northeastern, and southwestern built-up areas currently.

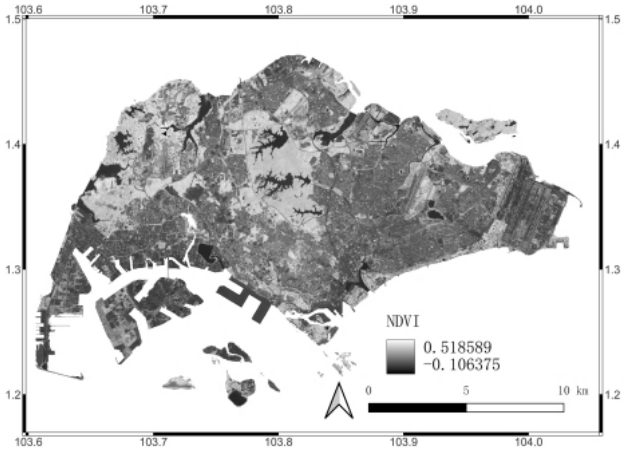

Figure 6. NDVI of the research site based on Landsat 8 satellite imagery.

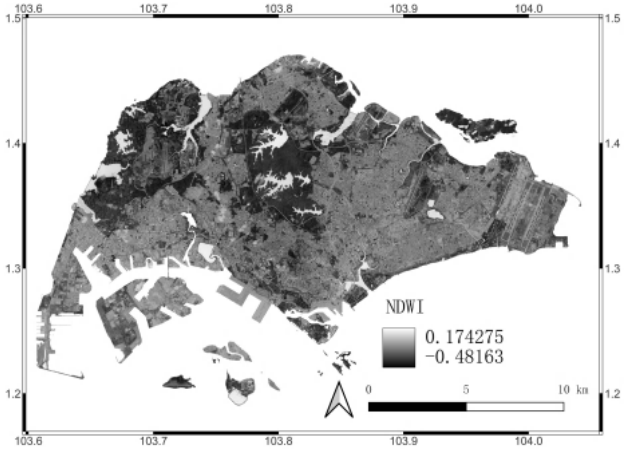

Figure 7. NDWI of the research site based on Landsat 8 satellite imagery.

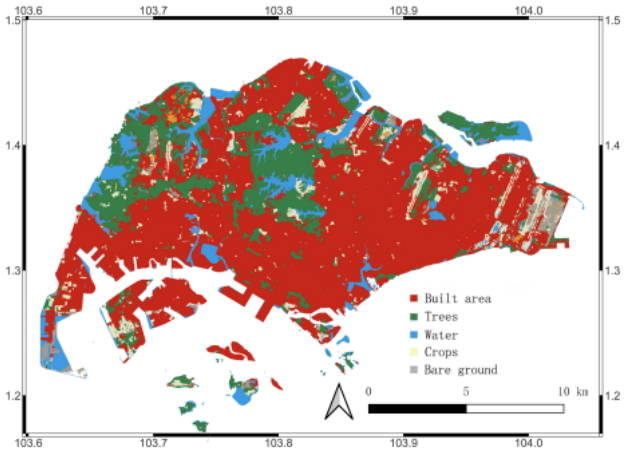

Figure 8. LULC of the research site in 2022 based on Sentinel-2 imagery.

4.3 Predicted UHS

The CNN model, which is trained based on current UHS and independent variables, has shown a test accuracy of 0.92 after seven epochs of training. Due to the high test accuracy of the

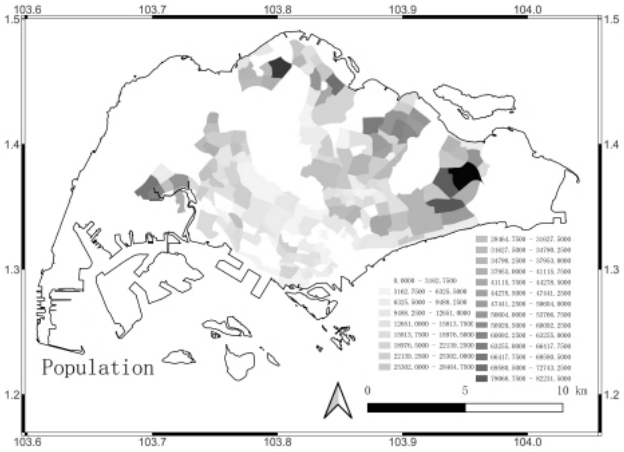

Figure 9. Current distribution of population of the research site.

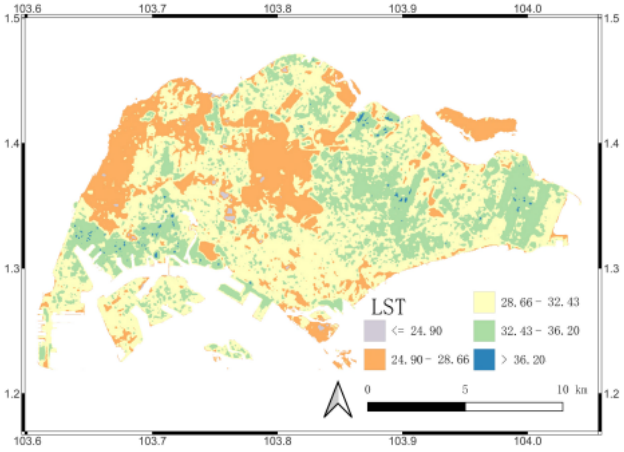

Figure 10. LST of the research site based on Landsat 8 satellite imagery. Unit: Celsius.

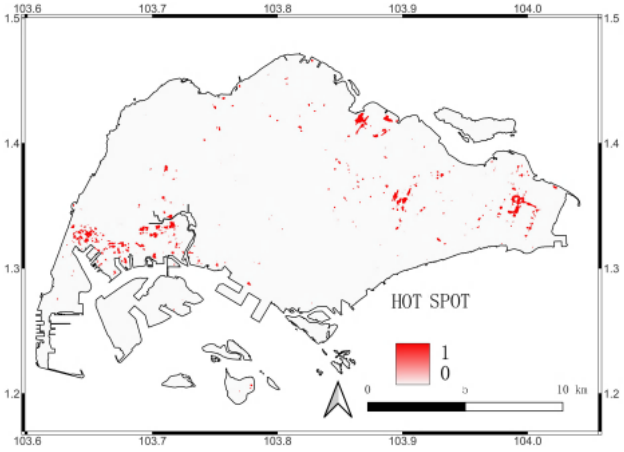

Figure 11. Current UHS of the research site.

trained model, this research uses the trained model along with its parameters to predict the future UHS of 2025. Feeding the predicted LULC of 2025 into the trained model, we generated the projected UHS for 2025, depicted in Figure 14. Quantitatively, compared to the existing UHS, as shown in Figure 11, where UHS occupies 0.95 percent of the entire research site, the predicted UHS, as shown in Figure 14, occupies 2.24 percent of the research site. From the image, it is observable that most of the UHS remains concentrated in the current UHS locations. However, more UHS are predicted in the southern areas, such as southwestern regions and Marina Bay, which were not evident in the current UHS diagram.

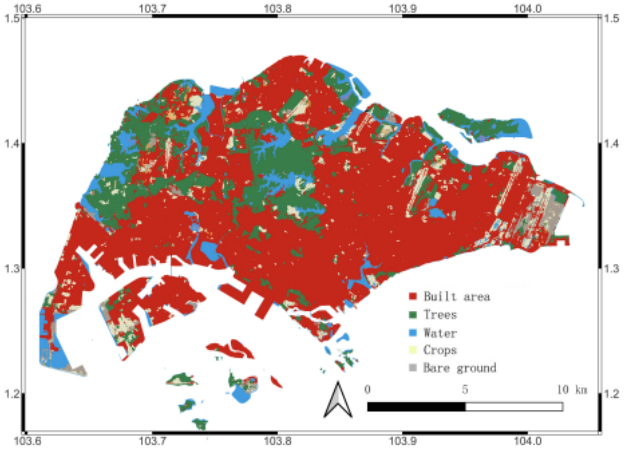

Figure 12. Projected LULC of the research site in 2025.

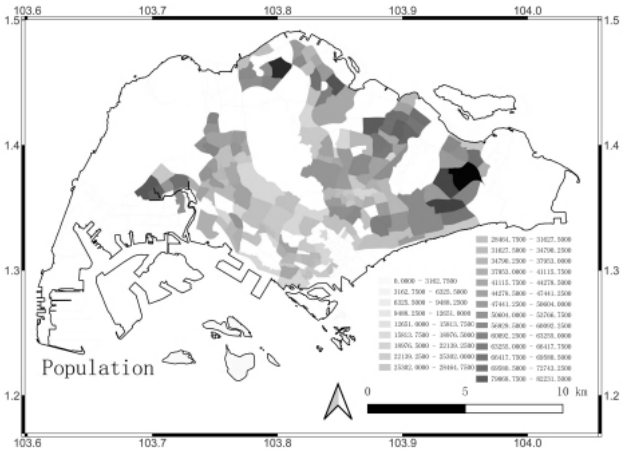

Figure 13. Projected population distribution in 2025.

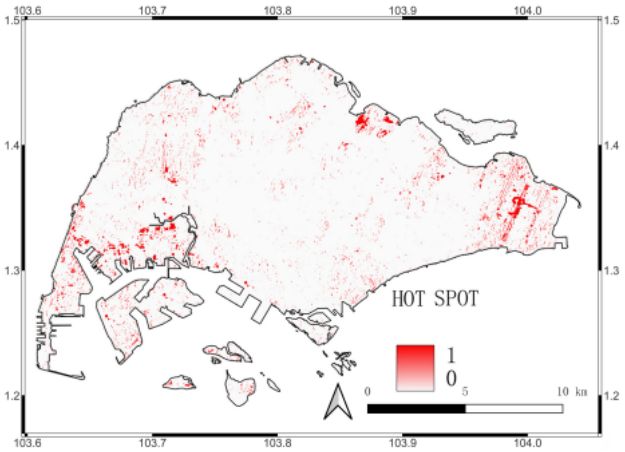

Figure 14. Predicted UHS of 2025 based on the CNN model.

This contribution has been peer-reviewed. The double-blind peer-review was conducted on the basis of the full paper.
https://doi.org/10.5194/isprs-annals-X-4-2024-195-2024 | © Author(s) 2024. CC BY 4.0 License.

5. Discussion

5.1 Potential UHS in the Future and Related Implications

As mentioned in Section 4.3, by comparing the existing UHS and projected UHS based on the CNN model, it is evident that the main locations of concentrated UHS remain unchanged. Specifically, most of the concentrated UHS are located near Changi Airport, and in the southwestern and northeastern parts of the country. The new projected UHS indicates that with the projected population and LULC, some new UHS will appear in the southwestern areas, Marina Bay area, and in northwestern areas. Research has investigated potential methods to lower LST and thus reduce UHS, and these measures could be potentially implemented according to our projected UHS to mitigate UHS effectively. For example, increasing the coverage of green spaces has been shown to be effective in lowering LST and reducing UHI (Li and Zheng, 2023). Thus, based on the predicted locations of UHS in this research, urban planners and designers could increase the amount of urban green spaces or implement other potential mitigation measures around predicted UHS areas to prevent the formation of UHS in advance. However, while implementing or increasing green space coverage in areas like parks is feasible, it is not practical in land used for specific industrial purposes. For instance, Changi Airport or oil refining centers in Jurong Island might not be allowed to renovated to incorporate more plants to reduce LST. In such instances, alternative measures, such as transitioning to pavement materials with high albedo values, could be adopted to reduce LST (Tahooni et al., 2023).

5.2 Limitations

There are a few limitations to this research. Firstly, the study identified seven independent variables related to LST values based on a literature review to project UHS. Additional factors could be added to the model to check if their inclusion improves the model’s accuracy. Secondly, when projecting future UHS, this research only updated the population and LULC variables, and the rest of the variables were not projected. Furthermore, master plans and future redevelopment plans from governmental agencies should be considered when projecting future values of variables. For example, the Greater Southern Waterfront plan, which will redevelop 2,000 hectares of land from Marina East to Pasir Panjang, will undoubtedly impact the current LULC of the research site. In future research, we intend to project future values for the remaining variables with greater precision to enhance the robustness of the projected UHS scenarios.

6. Conclusion

This research employs multiple independent variables that were identified by previous researchers as closely related to urban heat, including elevation, NDBI, NDMI, NDVI, NDWI, population, and LULC, along with the dependent variable, existing UHS distribution, to train the CNN model for predicting future potential UHS. By predicting LULC and population in year 2025, this study is able to predict the projected distribution of UHS. According to the results, the majority of projected UHS locations are the same as the current UHS. New UHS primarily appear in the southwestern areas, Marina Bay area, and the northwest areas of the country. Based on these projected locations, preventive measures are proposed in the research to mitigate UHS in advance. Compared to previous commonly used prediction methods whose feature data is collected at various points, such as weather stations (Liu et al., 2021; Alonso and Renard, 2020) in research sites, this study collects feature data from each pixel of images to predict values of UHS pixel by pixel, continuously. Urban planners and decision-makers could implement mitigation measures in advance at the newly identified UHS predicted by the model, thereby preventing the proliferation of UHS.

7. Acknowledgements

This research is partially conducted at the Future Cities Lab Global at Singapore-ETH Centre. Future Cities Lab Global is supported and funded by the National Research Foundation, Prime Minister’s Office, Singapore under its Campus for Research Excellence and Technological Enterprise (CREATE) program and ETH Zurich (ETHZ), with additional contributions from the National University of Singapore (NUS), Nanyang Technological University (NTU), Singapore and the Singapore University of Technology and Design (SUTD).

References

Ahmed, S., 2018. Assessment of urban heat islands and impact of climate change on socioeconomic over Suez Governorate using remote sensing and GIS techniques. *The Egyptian Journal of Remote Sensing and Space Science*, 21(1), 15–25.

Alonso, L., Renard, F., 2020. A New Approach for Understanding Urban Microclimate by Integrating Complementary Predictors at Different Scales in Regression and Machine Learning Models. *Remote Sensing*, 12(15), 2434.

Amindin, A., Pouyan, S., Pourghasemi, H. R., Yousefi, S., Tiefenbacher, J. P., 2021. Spatial and temporal analysis of urban heat island using Landsat satellite images. *Environmental Science and Pollution Research*, 28(30), 41439–41450.

Bokaie, M., Zarkesh, M. K., Arasteh, P. D., Hosseini, A., 2016. Assessment of urban heat island based on the relationship between land surface temperature and land use/land cover in Tehran. *Sustainable Cities and Society*, 23, 94–104.

Coutts, A. M., White, E. C., Tapper, N. J., Beringer, J., Livesley, S. J., 2015. Temperature and human thermal comfort effects of street trees across three contrasting street canyon environments. *Theoretical and Applied Climatology*, 124(1–2), 55–68.

Das, M., Das, A., 2020. Assessing the relationship between local climatic zones (LCZS) and land surface temperature (LST) – a case study of Sriniketan-Santiniketan Planning Area (SSPA), West Bengal, India. *Urban Climate*, 32, 100591.

Deo, R. C., Şahin, M., 2017. Forecasting long-term global solar radiation with an ann algorithm coupled with satellite-derived (MODIS) land surface temperature (LST) for regional locations in Queensland. *Renewable and Sustainable Energy Reviews*, 72, 828–848.

Equere, V., Mirzaei, P. A., Riffat, S., 2020. Definition of a new morphological parameter to improve prediction of urban heat island. *Sustainable Cities and Society*, 56, 102021.

Equere, V., Mirzaei, P. A., Riffat, S., Wang, Y., 2021. Integration of topological aspect of city terrains to predict the spatial distribution of urban heat island using GIS and ANN. *Sustainable Cities and Society*, 69, 102825.

Gao, B., 1996. NDWI—a normalized difference water index for remote sensing of vegetation liquid water from space. *Remote Sensing of Environment*, 58(3), 257–266.

Guha, S., 2017. Dynamic analysis and ecological evaluation of urban heat islands in Raipur City, India. *Journal of Applied Remote Sensing*, 11(03), 1.

Guha, S., Govil, H., Dey, A., Gill, N., 2018. Analytical study of land surface temperature with NDVI and NDBI using Landsat 8 OLI and TIRS data in Florence and Naples City, Italy. *European Journal of Remote Sensing*, 51(1), 667–678.

Halder, B., Bandyopadhyay, J., Banik, P., 2021. Monitoring the effect of urban development on urban heat island based on remote sensing and geo-spatial approach in Kolkata and adjacent areas, India. *Sustainable Cities and Society*, 74, 103186.

Huang, X., Wang, Y., 2019. Investigating the effects of 3D urban morphology on the surface urban heat island effect in urban functional zones by using high-resolution remote sensing data: a case study of Wuhan, Central China. *ISPRS Journal of Photogrammetry and Remote Sensing*, 152, 119–131.

Kardinal, S., Wong, N., Hagen, E., Anggoro, R., Hong, Y., 2007. The influence of land use on the urban heat island in Singapore. *Habitat International*, 31(2), 232–242.

Khalil, U., Aslam, B., Azam, U., Khalid, H. M. D., 2021. Time series analysis of land surface temperature and drivers of urban heat island effect based on remotely sensed data to develop a prediction model. *Applied Artificial Intelligence*, 35(15), 1803–1828.

Krtalić, A., Kuveždić Divjak, A., Čmrlec, K., 2020. Satellite-driven assessment of surface urban heat islands in the city of Zagreb, Croatia. *ISPRS Annals of the Photogrammetry, Remote Sensing and Spatial Information Sciences*, V-3–2020, 757–764.

Kuang, W., Liu, Y., Dou, Y., Chi, W., Chen, G., Gao, C., Yang, T., Liu, J., Zhang, R., 2014. What are hot and what are not in an urban landscape: quantifying and explaining the land surface temperature pattern in Beijing, China. *Landscape Ecology*, 30(2), 357–373.

Kumar, B. P., Babu, K. R., Anusha, B., Rajasekhar, M., 2022. Geo-environmental monitoring and assessment of land degradation and desertification in the semi-arid regions using Landsat 8 OLI / TIRS, LST, and NDVI approach. *Environmental Challenges*, 8, 100578.

Li, J., Li, Z., Lin, J., Li, K., Feng, G., 2023. A GIS-based approach to assess elderly liveability in Singapore and to suggest possible directions for optimization. *Proceedings of Building Simulation 2023: 18th Conference of IBPSA*, BS 2023, IBPSA.

Li, L., Tan, Y., Ying, S., Yu, Z., Li, Z., Lan, H., 2014. Impact of land cover and population density on land surface temperature: case study in Wuhan, China. *Journal of Applied Remote Sensing*, 8(1), 084993.

Li, Q., Zheng, H., 2023. Prediction of summer daytime land surface temperature in urban environments based on machine learning. *Sustainable Cities and Society*, 97, 104732.

Liu, J., Zhang, L., Zhang, Q., Zhang, G., Teng, J., 2021. Predicting the surface urban heat island intensity of future urban green space development using a multi-scenario simulation. *Sustainable Cities and Society*, 66, 102698.

Mcfeeters, S. K., 1996. The use of the normalized difference water index (NDWI) in the delineation of open water features. *International Journal of Remote Sensing*, 17(7), 1425–1432.

Muhammad, R., Zhang, W., Abbas, Z., Guo, F., Gwiazdzinski, L., 2022. Spatiotemporal Change Analysis and Prediction of Future Land Use and Land Cover Changes Using QGIS MOLUSCE Plugin and Remote Sensing Big Data: A Case Study of Linyi, China. *Land*, 11(3), 419.

Pearsall, H., 2017. Staying cool in the compact city: vacant land and urban heating in Philadelphia, Pennsylvania. *Applied Geography*, 79, 84–92.

Purevdorj, T., Tateishi, R., Ishiyama, T., Honda, Y., 1998. Relationships between percent vegetation cover and vegetation indices. *International Journal of Remote Sensing*, 19(18), 3519–3535.

Rajagopal, P., Priya, R. S., Senthil, R., 2023. A review of recent developments in the impact of environmental measures on urban heat island. *Sustainable Cities and Society*, 88, 104279.

Tahooni, A., Kakroodi, A., Kiavarz, M., 2023. Monitoring of land surface albedo and its impact on land surface temperature (LST) using time series of remote sensing data. *Ecological Informatics*, 75, 102118.

Taloor, A. K., Manhas, D. S., Chandra Kothyari, G., 2021. Retrieval of land surface temperature, normalized difference moisture index, normalized difference water index of the Ravi basin using Landsat data. *Applied Computing and Geosciences*, 9, 100051.

Voogt, J., 2008. How researchers measure urban heat islands. Unpublished article or working paper.

Wang, H., Yang, J., Chen, G., Ren, C., Zhang, J., 2023. Machine learning applications on air temperature prediction in the urban canopy layer: A critical review of 2011–2022. *Urban Climate*, 49, 101499.

Yuan, F., Bauer, M. E., 2007. Comparison of impervious surface area and normalized difference vegetation index as indicators of surface urban heat island effects in Landsat imagery. *Remote Sensing of Environment*, 106(3), 375–386.

Zeng, L., Lindberg, F., Zhang, X., Pan, H., Lu, J., 2023. Road surface temperature evaluated with streetview-derived parameters in a hot and humid megacity. *Urban Climate*, 51, 101585.

Zha, Y., Gao, J., Ni, S., 2003. Use of normalized difference built-up index in automatically mapping urban areas from TM imagery. *International Journal of Remote Sensing*, 24(3), 583–594.

Zhang, Y., Odeh, I. O., Han, C., 2009. Bi-temporal characterization of land surface temperature in relation to impervious surface area, NDVI and NDBI, using a sub-pixel image analysis. *International Journal of Applied Earth Observation and Geoinformation*, 11(4), 256–264.

Zhu, W., Yuan, C., 2023. Urban heat health risk assessment in Singapore to support resilient urban design — by integrating urban heat and the distribution of the elderly population. *Cities*, 132, 104103.